PROCEEDINGS OF SPIE

SPIEDigitalLibrary.org/conference-proceedings-of-spie

Main functions, recent updates, and applications of Synchrotron Radiation Workshop code

Oleg Chubar
Maksim Rakitin
Yu-Chen Chen-Wiegart
Yong S. Chu
Andrei Fluerasu
Dean Hidas
Lutz Wiegart

SPIE.

Main functions, recent updates and applications of "Synchrotron Radiation Workshop" code

Oleg Chubar*[a], Maksim Rakitin[a], Yu-chen Karen Chen-Wiegart[a], Yong S. Chu[a], Andrei Fluerasu[a], Dean Hidas[a], Lutz Wiegart[a]
[a]National Synchrotron Light Source II, Brookhaven National Laboratory, NY, USA 11973

ABSTRACT

The paper presents an overview of the main functions and new application examples of the "Synchrotron Radiation Workshop" (SRW) code. SRW supports high-accuracy calculations of different types of synchrotron radiation, and simulations of propagation of fully-coherent radiation wavefronts, partially-coherent radiation from a finite-emittance electron beam of a storage ring source, and time-/frequency-dependent radiation pulses of a free-electron laser, through X-ray optical elements of a beamline. An extended library of physical-optics "propagators" for different types of reflective, refractive and diffractive X-ray optics with its typical imperfections, implemented in SRW, enable simulation of practically any X-ray beamline in a modern light source facility. The high accuracy of calculation methods used in SRW allows for multiple applications of this code, not only in the area of development of instruments and beamlines for new light source facilities, but also in areas such as electron beam diagnostics, commissioning and performance benchmarking of insertion devices and individual X-ray optical elements of beamlines. Applications of SRW in these areas, facilitating development and advanced commissioning of beamlines at the National Synchrotron Light Source II (NSLS-II), are described.

Keywords: synchrotron radiation, X-rays, insertion devices, physical optics, computer simulations

1. INTRODUCTION

Computer simulation codes play currently a decisive role in the development of modern light source facilities – storage ring based synchrotron radiation sources and linac based free-electron lasers. High-accuracy simulations by particle-tracking accelerator physics codes (see e.g. [1], [2]) greatly contributed to the progress made over the recent years in reduction of electron beam emittance in electron storage rings, down to ~100 pm level, and, as a consequence, very impressive increase of brightness of light sources based on these rings [3] - [5]. Simulation of multi-particle dynamics and impedance-related effects based on numerical solution of the associated electrodynamics problems in 2D and in 3D [6] facilitate detailed optimization of vacuum, RF, injection systems of these accelerators, and, as a result, enable stable operation of modern storage ring based sources at a high (~0.5 A in medium energy rings) average electron current, and the corresponding high average flux of the output Synchrotron Radiation (SR).

However, accelerator physics codes are not sufficient for the design and optimization of modern light source facilities. A very important place in the panoply of the software addressing these purposes is taken by the high-accuracy 3D magnetostatics codes dedicated for magnetic design of Insertion Devices (IDs) – undulators and wigglers – producing the radiation [7], and the electrodynamics codes that can accurately calculate all key characteristics of the SR generated by relativistic electrons in these magnetic fields [8] - [11]. A detailed knowledge of the SR characteristics is nevertheless still not sufficient for making use of this radiation in experiments. The emitted radiation has to be transported to experimental samples by optical systems of beamlines that have to be optimized and be of sufficient quality to not deteriorate important characteristics of the radiation beams, such as brightness and coherence, during this transport. The radiation transport, or propagation through individual optical elements and spaces in a beamline, has therefore to be simulated in detail, and this simulation has to be used as a basis for the optical system optimization prior to its practical realization.

The modern light source facilities – ultra-small electron beam emittance storage rings and, even more so, free-electron lasers – produce significant portions of coherent radiation, even at very small wavelengths belonging to hard X-ray range, and further increase of the radiation degree of coherence represents one of the main strategic goals for future development of these sources.

*chubar@bnl.gov; phone 1 631 344-4525; fax 1 631 344-8189; www.bnl.gov

Advances in Computational Methods for X-Ray Optics IV, edited by Oleg Chubar, Kawal Sawhney, Proc. of SPIE Vol. 10388, 1038805 · © 2017 SPIE
CCC code: 0277-786X/17/$18 · doi: 10.1117/12.2274285

To enable accurate simulation of the processes taking place during the propagation of such fully- or partially-coherent radiation, the software that is used for such simulation has to be based on the principles of physical optics. We note that this requirement was much less important for earlier generations of synchrotron / storage ring based light sources, in which, because of a large electron beam emittance, the generated SR was much less coherent for the most part of spectrum, and therefore could be in general adequately simulated by software using the approximation of geometrical optics [12] - [14]. Recently, efforts were made to extend the proven and popular geometrical ray-tracing codes, such as SHADOW [12], to simulate wave-optics phenomena "only were necessary", while remaining within the geometrical optics approximation for the most part of an X-ray beam transport simulation [15]. Even though this approximate approach was demonstrated to give correct results in some special cases of beamlines (e.g. with one secondary source aperture), it has, from our point of view, several important weaknesses, such as a necessity to make assumptions about radiation phase when extrapolating it from intensity, and a strongly increasing numerical complexity of the simulation when effects of diffraction at a number of apertures along the beam path have to be taken into account, in particular in a 2D simulation case.

In this paper we briefly describe the electrodynamics and physical optics based methods and functions implemented in the SRW synchrotron emission and radiation propagation simulation code, and present examples of simulations performed recently using this code. The SRW code operates with two orthogonal transverse polarization components of the frequency-domain complex electric field when calculating SR and simulating its propagation. To describe emission by an individual electron, a classical electrodynamics method based on retarded potentials is used; for the simulation of propagation, methods of physical optics are employed. To accurately describe the emission and propagation of partially-coherent SR beam, a method based on averaging over the phase-space volume of the emitting electron beam is used, taking into account that the emission by different electrons in a storage ring is not correlated for the most part of the SR spectrum. This approach has clear advantages in terms of accuracy, generality, and, at the same time, relative simplicity of implementation. With this approach, all the simulations are done at the same (high) accuracy level; no assumptions about a source, no extrapolation or conversion of the radiation characteristics or representation at different simulation steps are required. The "price to pay" with this approach is, however, a potentially long computation time required for the cases of low radiation coherence. This disadvantage can be overcome e.g. by parallel calculations and / or by using convolution-based techniques where possible.

The simulation examples to be presented will cover both the processes of emission and propagation of the radiation through beamline optics. All these examples are related to development, commissioning and / or operation of the NSLS-II low-emittance storage ring SR source that has been recently constructed at Brookhaven National Laboratory, USA.

2. OVERVIEW OF THE MAIN SRW FUNCTIONS

2.1 High-accuracy calculation of synchrotron radiation (spontaneous emission) characteristics

The main SR calculation method implemented in the SRW code is based on the retarded potentials technique and allows for high-accuracy CPU-efficient computation of the horizontal and vertical components of the frequency-domain SR electric field generated by a relativistic electron in a magnetic field of arbitrary configuration as observed in the near-field region [9], [16]. The exact expression for the frequency-domain near-field electric field used in this method (see Eq. (1) in [9] and [16]) is easily derived using analytical representation of delta-functions in the scalar and vector retarded potentials by Fourier integrals and subsequent analytical differentiation (as necessary for deriving the electric field from the potentials). To accelerate numerical calculation according to this expression, its asymptotic expansion at limits of an integration interval along an electron trajectory can be used.

This method can be effectively used e.g. for high-accuracy calculation of single-electron radiation from planar and elliptically-polarizing undulators, taking into account magnetic field errors and effects of terminations, radiation from few-pole and multi-pole wigglers (taking into account eventual interference effects), radiation from central parts and edges of bending magnets, miscellaneous short magnets, and even quadrupole and sextupole magnets (for electrons moving off their axes). In the most general case of an arbitrary 3D magnetic field configuration, the electron trajectory, which is required for the SR computation, is calculated using the 4th order Runge-Kutta method. In a simpler case of an ultra-relativistic electron moving in a transversely-uniform 2D magnetic field, the trajectory is calculated using integration of the magnetic field along the longitudinal position.

The single-electron SR spectral flux per unit surface area (that we often reference below as "intensity") in a given observation plane is proportional to the squared amplitude of the frequency-domain electric field in that plane. The intensity of SR produced by a finite-emittance electron beam is calculated in SRW by averaging the single-electron

intensity over the phase-space volume occupied by this beam [17]. The same general method can be used for the calculation of mutual intensity (or cross-spectral density), which in turn can be used to accurately calculate the radiation degree of coherence.

Besides the high-accuracy near-field calculation of monochromatic SR, the code supports power density calculations at observation points in the near and far field, at an arbitrary orientation of an observation plane (not necessarily perpendicular to the emission axis). This method can be used to estimate heat load produced by the SR from bending magnets and IDs on internal surfaces of vacuum system components, absorbers and first optical elements of beamlines.

In addition to the high-accuracy near-field SR calculation methods, SRW also supports several approximate (but fast) SR calculation methods. One of such methods is the estimation of spectral brightness of synchrotron (/ undulator / wiggler / bending magnet) radiation. For the estimation of Undulator Radiation (UR) brightness, besides the electron beam transverse emittance, impacts from the electron beam energy spread, and a possible "detuning" of photon energy with respect to resonant value of an UR harmonic can be taken into account. Another practically-important approximate method implemented in SRW enables fast calculation of UR spectral flux (within a fixed aperture or per unit surface area), taking into account finite electron beam emittance. The undulator magnetic field is assumed to be perfectly periodic (but not necessarily sinusoidal) of a finite length, and the observation is assumed to be in the far field in this method. The method is similar to the one used by the popular URGENT code [8], except that it efficiently takes into account the electron beam energy spread.

2.2 Simulation of fully-coherent radiation propagation through optical systems

Another very important part of the SRW code is dedicated to the simulation of fully-coherent radiation propagation through optical components and drift spaces separating them in a beamline. The simulation of propagation of a fully-coherent radiation beam is implemented using a combination of the CPU-efficient Fourier optics, the stationary phase, and the X-ray dynamical diffraction based methods. For each optical element and drift space, the propagation of two transverse components of the frequency-domain electric field is simulated locally, from a plane perpendicular to the optical axis before the element, to a plane perpendicular to the optical axis after it.

The Fourier optics "propagators" are used first of all for drift spaces. Several such propagators are available in the code. Two general ones simulate propagation of the electric field between parallel planes by calculating the convolution-type Fresnel integral in the small-angle approximation using two 2D Fast Fourier Transforms (FFT), without and with a semi-analytical treatment of the quadratic phase term to reduce memory requirements [18]. Special drift space propagators based on one 2D FFT are available to efficiently simulate the electric field propagation over a large distance from or to a waist position. The Fourier optics type processing is also used for optical elements and effects that can be simulated by multiplication of the transverse electric field components by a complex transmission function (which can possibly be different for each of the two field components): refractive and diffractive optics, apertures, miscellaneous masks, phase shifts varying over transverse position due to reflection from imperfect mirrors, perfect mirrors in "thin element" approximation, etc. A combination of the drift space and transmission function type propagators can be used to simulate some types of longitudinally-extended optical elements, e.g. a Compound Refractive Lens (CRL) with a large number of individual lenses installed consecutively.

A special stationary-phase method based propagator is available for simulation of longitudinally-extended mirrors, which are used at small incident angles in the soft and hard X-ray range, and also for gratings, that are the key elements of monochromators for soft X-rays. The mirror / grating reflectivity can be different for different transverse electric field components, and it can affect both the amplitudes and phases of these components. The numerical transformation of the electric field components due to reflection is done in the local frame of the mirror. The electric field is propagated "along rays", according to the first term of the stationary phase approximation of the Kirchhoff integral, to an output plane perpendicular to the optical axis of the reflected beam "at the exit" of the mirror / grating. The "reflection laws" are different in the cases of mirrors and gratings; and in the case of a grating, the electric field obtains an eventual extra phase shift that depends on the diffraction order and is calculated according to the grating relation. After the electric field is obtained in the output plane in the frame of the output beam, it is re-sampled on a regular mesh vs. "horizontal" and "vertical" positions in that frame, using 2D interpolation (the re-sampling is required to make sure that further propagation of the resulting electric field can be made using methods involving 2D FFT). This propagator assumes that no diffraction effects take place when the beam is reflected from the central part of the mirror / grating. If necessary, diffraction at mirror / grating edges can be simulated using the Fourier optics methods, applied in addition to the stationary-phase propagator.

For simulation of hard X-ray monochromators within the framework of physical optics, dynamical diffraction theory based propagators for perfect crystals in the Bragg geometry for reflected and transmitted beams, were added to SRW [19]. These propagators use Zachariasen's formulae [20] for transforming the electric field components. To be able to apply these formulae, the frequency-domain electric field components need to be in the angular representation (so a conversion from the spatial to the angular representation may need to be done by means of a 2D FFT) and transformed to the local crystal frame (from the frame of the incident beam). After applying the formulae, another spatial transformation is used to bring the electric field components to the frame of the output beam, and, as in the case of the stationary-phase propagator, the electric field is re-sampled, using 2D interpolation, on a regular mesh vs. "horizontal" and "vertical" positions in the plane perpendicular to the optical axis of the output beam. Finally (if necessary) an inverse 2D FFT can be done to obtain the electric field in the spatial representation. This propagator can be used for symmetrically- and asymmetrically-cut crystals.

The panoply of propagators for different types of X-ray optical elements available in SRW allows for realistic physical optics based simulation of propagation of coherent X-ray beams through beamlines of very high complexity, dedicated to different types of experiments. Nevertheless, a few propagators, for less common types of X-ray optics, are still planned to be implemented, or the work on their implementation in SRW is currently in progress. One of such propagators will support simulation of radiation propagation through crystals in Laue geometry, the other will support simulations with multilayer Laue lenses that are very successfully used at the Hard X-ray Nanoprobe (HXN) beamline at NSLS-II [21]. Work is also currently in progress on improving the accuracy of simulations of imperfect mirrors and refractive optics, and benchmarking the results of such simulations against measurements at X-ray beamlines.

The main advantage of using the Fourier optics and compatible methods for the simulation of coherent radiation propagation is the high CPU-efficiency of these methods (compared to other known physical optics methods). However, the FFT based Fourier optics "apparatus" somewhat lacks numerical robustness and "stability", especially in cases when the radiation beam is strongly changing its spatial dimensions and / or angular divergences and / or wavefront curvature in the process of propagation. To enable keeping a required level of numerical accuracy at such simulations, SRW code has functions for resizing / resampling of the radiation electric field that can be applied at any step of the propagation. These functions use the 2D interpolation and / or "padding zeros" method applied to the electric field distribution either in the spatial or in angular representation. However, for users of the code who do not have previous experience with the methods of Fourier optics or FFT apparatus, the choice of optimal electric field resizing / resampling parameters for simulating of radiation propagation through a given optical system usually represents difficulties. Because of this, work is in progress on implementing a general propagation "driver" capable of "automatic" choice and steering of these parameters at each propagation step based on analytical estimations and "pre-propagations" of 1D cuts of the radiation electric field. The robustness of simulations was also significantly improved after implementation of special drift space propagators, in particular the one performing semi-analytical treatment of the quadratic phase term. Further work on improving this propagator is also currently in progress.

The SRW functions described in this section allow for high accuracy and high CPU-efficiency simulation of propagation of ~fully coherent radiation beams or pulses, such as those of an X-ray free electron laser, in steady-state or in time- / frequency-dependent mode [22], [23]. However, for high-accuracy simulation of propagation of partially-coherent radiation through beamlines of a storage-ring based SR source, several more functions had to be added to the code. These functions are described in the next section.

2.3 Simulation of partially-coherent radiation propagation

The method for simulation of partially-coherent radiation propagation through a beamline of a storage ring based SR source in the SRW code makes use of the fact that spontaneous emission by different electrons of a bunch circulating in a storage ring is uncorrelated (i.e. is temporally incoherent) at the wavelengths smaller than the bunch length – that means for the most part of the SR spectrum used in experiments. On the other hand, the radiation by one electron is fully coherent, and its propagation through an optical system can therefore be accurately simulated using the methods described in the previous section. In such a situation, the intensity (and / or mutual intensity) of the radiation from the entire electron beam after the propagation through an optical system can be calculated by summing up (mutual) intensities derived from electric fields emitted by different electrons and propagated through this optical system. For such calculation, initial conditions defining trajectories of these electrons have to be distributed over the entire 6D or 5D (if time dependence is not important) phase space occupied by the electron beam. The practical realization of this calculation method is simple – one just has to "loop" over single-electron SR electric field calculation and its propagation (using the functions described in the previous two sections) at different initial transverse positions and angles of the electron trajectory at different electron energy values, seeded according to some distribution (usually Gaussian, which accurately represents a "damped" electron beam in a

storage ring), and to sum-up the resulting (mutual) intensities after each propagation. If the simulation has to be performed for polychromatic SR within a finite bandwidth, e.g. in the presence of a monochromator among other optical elements, one more integration variable, photon energy, has to be added to this integration over the phase space of the "source".

Thanks to the simplicity of implementation of this calculation method for the partially-coherent SR emission and propagation and thanks to its potentially high accuracy, it started to be used in the SRW code since quite some time (shortly after the first releases of the code [24]), and allowed to obtain a number of very useful results in the areas of electron and X-ray beam diagnostics [24], [25], and SR beamline optimization for a new low-emittance synchrotron source [26], [27].

This method, however, has an important disadvantage: it is very CPU intensive, in particular in cases when the electron beam emittance is large and coherence of the emitted radiation is poor, and the integration over the phase space volume of the electron beam cannot be accelerated using a convolution-type relation. Indeed, even if the simulation of emission and propagation of radiation from one electron takes seconds, repeating such simulation sequentially hundreds of thousands of times will result in a calculation lasting many days. Fortunately, this type of calculation can be also very easily parallelized and therefore can run much faster on a multi-core server or a small / medium size computer cluster. The required calculation time in such a case can be reduced nearly proportionally to the number of processor cores used, i.e. can be easily reduced by factor of 10-100 or more on an easily-accessible computer system.

We also note that with this calculation method, the smaller is the emittance of the electron beam, and so the higher is the degree of coherence of the produced radiation, the smaller is the calculation time required for high-accuracy simulation of its emission and propagation. This means that for any new generation of storage ring based SR sources, the calculation of the emission and propagation of the partially-coherent radiation produced by them is faster and faster with this method. Nevertheless, despite of these considerations and besides the use of parallel computing, attempts to accelerate this type of calculation, using several different approaches, are currently underway.

3. SRW IMPLEMENTATION AND INTERFACES

The most important core part of the SRW code is written in C++. This part contains the implementation of the main algorithms for the electron trajectory and SR calculation, for the simulation of fully-coherent radiation propagation through optical elements, and for miscellaneous manipulations with the radiation electric field (resizing / resampling, "extraction" of intensity at different polarizations from the electric field components, etc.). The code uses the FFTW prime-factor discrete Fourier transform library [28] for performing 1D and 2D FFTs (mainly in the propagation-related functions). The SRW library has a documented C-style Application Programming Interface (API), which allows for easy interfacing to any application / front-end supporting extension by shared or static libraries written in C/C++. After the transition of the SRW code to open source, all C/C++ source files were published on GitHub [29] along with interface-related files, simulation examples and other resources.

The very first versions of the SRW code were using the IGOR Pro package from WaveMetrics [30] as a front-end. The interface-related functions, dialogs, some pre- and post-processing was written in the IGOR macro-language. These versions of SRW are available from the ESRF web site [31]. The SRW for IGOR Pro for is still supported [29].

The SRW library was then interfaced to Python, using the Python C API [32]. Currently, the SRW can be used both with Python 2.7x and 3.x [33]. Besides the shared library, the Python-interfaced version of SRW has several Python modules that contain definitions of all SRW-related classes (magnetic field sources, X-ray optics, radiation electric field and Stokes components) and a number of functions supporting SRW simulations. One of such functions does parallel calculation of partially-coherent SR emission and propagation by the method described in the previous sections, using the Message Passing Interface (MPI), via the "mpi4py" Python module [34]. This function makes calls to functions of the SRW shared library for single-electron emission and propagation calculations. This SRW version contains a set of simulation examples, and also a "virtual beamline" Python module that simplifies definition of ID and X-ray optics parameters of beamlines at light sources and streamlines main types of calculations required for such beamlines.

Recently a new, web-based, interface – Sirepo – considerably simplifying server-side calculations with SRW for beamlines at light sources has been developed [35]. The application supports calculations on an individual server or on a computer cluster, potentially benefiting from cloud-computing services. On the client side, simulations can be started and controlled from any browser via a powerful graphical user interface implemented in JavaScript. This web interface can be easily used not only by beamline / instrumentation staff, but also eventually by users of light source facilities. Besides Sirepo, another web-based interface, using the IPython / Jupyter Notebook server [36] was developed at the European XFEL [37].

4. CALCULATION EXAMPLES: SR SOURCES

In this section, we present two examples of detailed simulations with SRW code dedicated to IDs that are used in modern low-emittance storage ring based light sources. These examples demonstrate the accuracy and generality of the methods implemented in the code, which enable a large number of applications in the area of development, commissioning and regular use of radiation sources.

4.1 Simulation of misalignment effects and spectrum-based alignment of in-vacuum undulators

Small-period and small magnetic gap In-Vacuum Undulators (IVU) are currently the main high-brightness and high-flux sources of hard X-rays in medium-energy storage rings. The technologies of production of this type of devices – pure permanent magnet and hybrid, room-temperature as well as cryo-cooled – are currently in a relatively mature state. Because of a typically large number of magnetic periods in these devices and a necessity to use high harmonics of their radiation in the medium-energy rings, special efforts are usually dedicated to their shimming to compensate magnetic errors, ensure good spectral performance and absence of adverse effects on electron beam dynamics. After installation of these IDs into a storage ring, they usually undergo a thorough commissioning from the point of view of accelerator physics (to minimize / eliminate beam lifetime reduction, set up good compensation of residual field integrals at any gap by "feed-forward" systems, etc.). However, with rare exceptions [38], [39], much less efforts are usually dedicated to benchmarking of real undulator spectral performances at beamlines. Even though software tools for calculation of UR spectra exist since quite some time [8] - [10], the use of these tools requires installation and some learning; it is also important to use correct input parameters for calculations, which may not be immediately known. The new Python and web-based interfaces of the SRW code [33], [35], and "virtual beamlines" that were implemented in these interfaces in strict correspondence with parameters of IDs and X-ray optics of real beamlines, considerably improved the availability and ease of use of such simulation tools by beamline staff and users of NSLS-II. This greatly helped to address the problems described below.

A very first comparison of measured and calculated UR spectra (flux per unit surface area) produced by a 21 mm period 1.5 m long IVU at the Submicron Resolution X-ray spectroscopy (SRX) beamline of NSLS-II made it clear that the spectral widths of the measured UR harmonics are considerably larger (by factor of ~2) than the corresponding harmonic widths in the calculated spectrum, see graph on the left in figure 1. Initial calculations were done assuming an error-free magnetic field. However, consecutive SRW calculations performed using the magnetic field measured in this IVU before installation, produced quite similar results, strongly different from the measurements. The significant discrepancy between the measured and calculated spectra motivated further numerical simulations and search for possible explanations. It was decided to simulate possible effects of modulation of undulator magnetic field "seen" by electrons. The results of these calculations, made in assumption of a linearly-modulated magnetic field, are also shown in figure 1. These calculations suggested that the measured large harmonic width value could possibly be explained by the magnetic field modulation making the peak field between undulator entrance and exit different by 1 - 1.5%. Besides this, the calculations clearly showed that the effect of the harmonic broadening is associated with the loss of peak spectral flux (per unit surface area and / or integrated within an aperture) at harmonics, see graph on the right in figure 1.

As a part of subsequent numerical analysis, UR spectra were calculated with the SRW code using the measured IVU magnetic field modified using a parametric relation derived from the well-known Halbach formula [40] with coefficients obtained from magnetic measurements and 3D magnetic calculations made with RADIA [7]. This relation allows for predicting the effects on the magnetic field from geometrical gap taper and / or angular or positional misalignment of the undulator magnet arrays with respect to the electron orbit trajectory. In these simulations, the undulator misalignment cases were chosen in an attempt to reproduce the imperfect UR spectrum measured at the 5th harmonic at 6.8 mm gap of the SRX IVU. The calculations were done for the NSLS-II operation mode with the gap of one (out of three) damping wigglers closed, which resulted in the horizontal electron beam emittance of 1.45 nm and the relative RMS electron energy spread of ~0.72×10^{-3}. The left graph in figure 2 shows the results of these simulations. As one can see from this graph, a quite realistic IVU misalignment case combining linear magnetic gap taper characterized by Δg = 50 μm gap difference between the IVU exit and entrance, vertical offset of the magnet girders by Δh = -235 μm, and vertical angular tilt of the magnet girders θ = 145 μrad results in the increase of the UR harmonic width by factor of ~2 and a reduction of the on-axis peak spectral flux by the same factor. A very similar effect, in terms of the measured harmonic width and shape (as compared to simulations for perfectly aligned undulator) was observed at the SRX beamline. The simulation results in the left graph in figure 2 also show that if $\Delta g = \Delta h = 0$, the IVU tilt angle θ = 145 μrad alone does not have any significant impact on the spectral performance. Based on these simulations, a strategy for improving the IVU spectral performance, consisting in a correction of the gap taper and steering the IVU position with respect to the electron beam, was chosen.

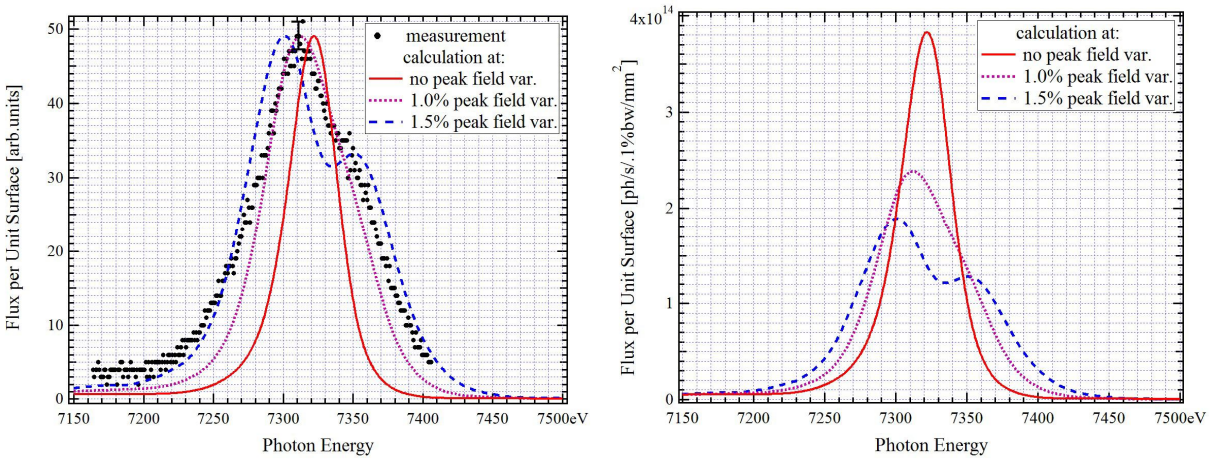

Figure 1. Left: on-axis UR spectral flux per unit surface area at 5th harmonic as function of photon energy measured at the SRX beamline at ~6.4 mm undulator gap (dots) and the corresponding calculations, performed based on measured magnetic field without and with linear taper-type modulation applied to it; the calculation results are normalized by a value that is close to the maximum of the measured curve. Right: same calculation results as on the left, plotted in absolute units, for the detector location (~37.4 m from the IVU center).

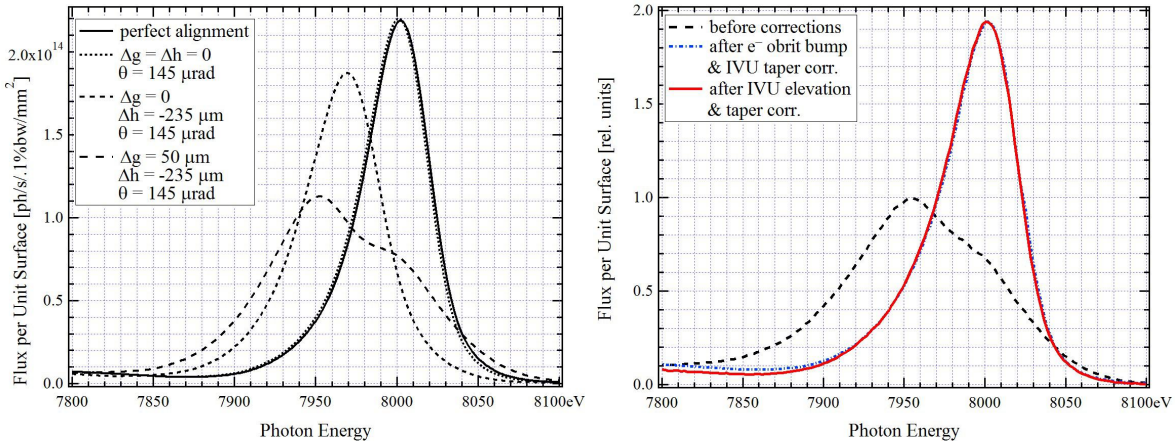

Figure 2. Left: calculated on-axis spectral flux per unit surface area at ~33 m observation distance at the 5th harmonic of a perfectly aligned IVU of the SRX beamline (solid line) and for different cases of misalignment (dotted / dashed lines), at ~6.8 mm average gap value. Right: on-axis UR spectral flux per unit surface area from the same IVU at the same harmonic and gap, measured before and after the spectrum based alignment by two different methods, with and without using vertical shift of electron orbit.

The tests of the IVU spectral performance at different (mis-)alignment of its magnet girders with respect to the average electron beam trajectory were done during a dedicated low-current accelerator operation, benefiting from the possibility of a remote independent adjustment of magnet girder positions and orientations in this undulator. These studies confirmed the factor of ~2 decrease of UR harmonic width and factor of ~2 increase of the peak on-axis spectral flux when the ~50 μm gap taper and -250 μm vertical parallel electron orbit "bump" were applied simultaneously, see graph on the right in figure 2. The same effect was reproduced when, instead of the vertical bump of the electron trajectory, the vertical "elevation" of the IVU magnet girders was changed. The optimal difference in the "elevation" was found to be close to the optimal electron orbit shift value determined previously by simulations and by measurements with the electron orbit bump (except that the direction of the "elevation" change had to be opposite to the orbit shift). The measured spectral flux per unit surface curves corresponding to these two corrections are almost indistinguishable from each other. After the spectrum-based alignment, the harmonic width in the measured UR on-axis flux per unit surface is by only ~10% larger than the prediction of the simulations assuming perfect IVU alignment. This can possibly be explained by a detector (YAG screen) effect.

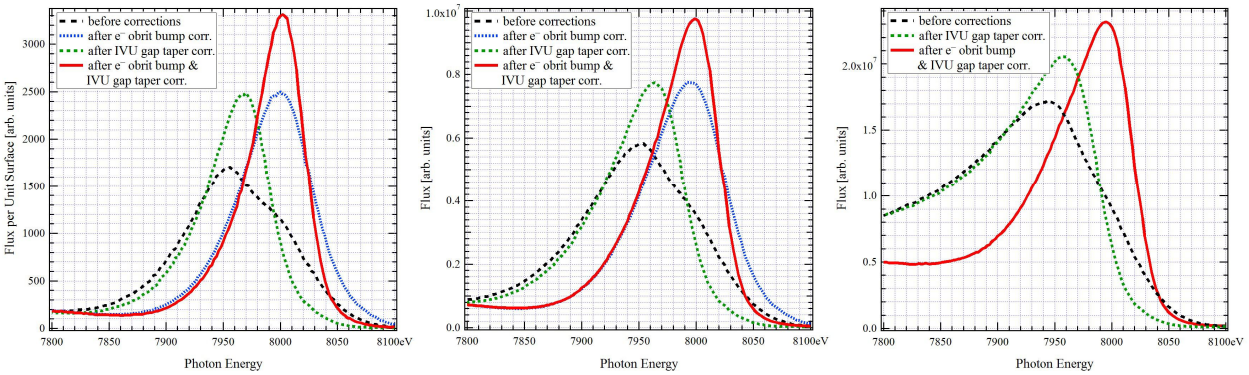

Figure 3. IVU21 spectral flux per unit surface area (left), spectral flux through a nominal 40 x 40 μrad^2 aperture typically used for experiments (middle), and through a very large 130 x 130 μrad^2 aperture that cannot be used for experiments because of X-ray optics dimensions limit (right) measured at the SRX beamline in the process of the spectrum-based alignment (using the method involving the electron orbit bump and the IVU gap taper correction).

Besides the on-axis spectral flux per unit surface area, the spectral flux within two different finite apertures was measured in the process of the spectrum based IVU alignment. The results of these measurements are presented in figure 3. These results demonstrate that a considerable, factor of ~1.7, gain in flux was obtained also for the aperture value that is typically used in experiments at the SRX beamline (see middle graph in figure 3). It was decided to leave the optimal settings of the magnetic gap taper and the girder elevation, found during this study, for everyday use in the IVU at the SRX beamline. After the successful spectrum based IVU alignment at the SRX beamline, the undulator spectral performance benchmarking against simulations is performed at every hard X-ray beamline using IVU at NSLS-II. By the time of this writing, the spectrum based alignment procedure was applied to 4 different IVU (out of 8 currently in use) and resulted in considerable spectral flux gains for the corresponding NSLS-II beamlines.

4.2 "Few-pole" wigglers replacing bending magnet sources in low-emittance storage ring based light sources

A known "side effect" of magnet lattice optimization to reduce emittance in modern storage-ring based light sources is the reduction of magnetic field in bending magnets. E.g. at NSLS-II, the magnetic field in central parts of bending magnets is ~0.4 T, whereas in the old second-generation NSLS X-ray ring it was ~1.4 T, and that ring had a large number of the bending-magnet based hard X-ray beamlines producing high-quality scientific results. This was (/is) also the case in a large number of currently operating 3rd generation storage ring sources. The on-going or planned upgrades of these storage rings to ultra-low emittance light sources [4], [5] requires therefore creation of special IDs that would be used as radiation sources for such bending magnet type beamlines. The NSLS-II solution to this problem consisted in development and production of a number of short hybrid permanent magnet 3-Pole Wiggler (3PW) devices that can be installed near bending magnet edges in the dispersion straight sections of the storage ring [41]. Such devices can easily produce relatively high (> 1 T) peak magnetic field in the central pole at relatively large (20 - 40 mm) magnetic gap. An advantage of using such devices is that they can be easily made to have zero first and second magnetic field integrals, i.e. their installation does not have a significant impact on the electron beam closed orbit, and so on "source points" and emission axes of other pre-existing / operating beamlines in a storage ring. However, these devices are more complicated than bending magnets, and have some features in spectral-angular distributions of radiation generated by them, that need to be taken into account for the development of the corresponding X-ray beamlines. In this section, we illustrate these features by SRW calculations. Most of these calculations were initially done during the development stage of NSLS-II, using modeling 3PW magnetic fields – to support the decision-making process about the use and design of the 3PW. The spectral calculations described in this section were updated using the measured magnetic fields of the NSLS-II 3PW and bending magnets.

A typical vertical magnetic field distribution as a function of longitudinal position along axis of a dispersion straight section of NSLS-II with a 3PW installed is shown in figure 4 (upper graph), together with the corresponding average electron trajectory (horizontal angle and position vs. longitudinal position). At the trajectory calculation, the initial conditions, namely, zero horizontal position and angle, were set in the 3PW center. The results of SR calculations described below were made for this magnetic field distribution (including the 3PW and the edges of bending magnets limiting the straight section) and this average electron trajectory.

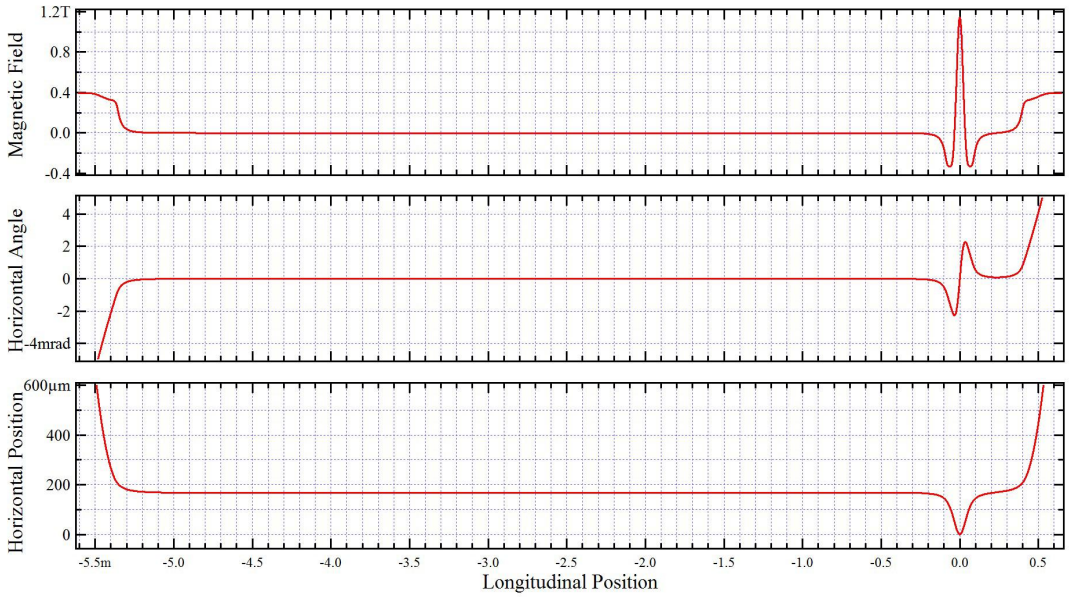

Figure 4. On-axis magnetic field (top), horizontal angle (middle) and horizontal position (bottom) of the average electron trajectory in the dispersion section of NSLS-II with a 3PW installed and bending magnet edges included.

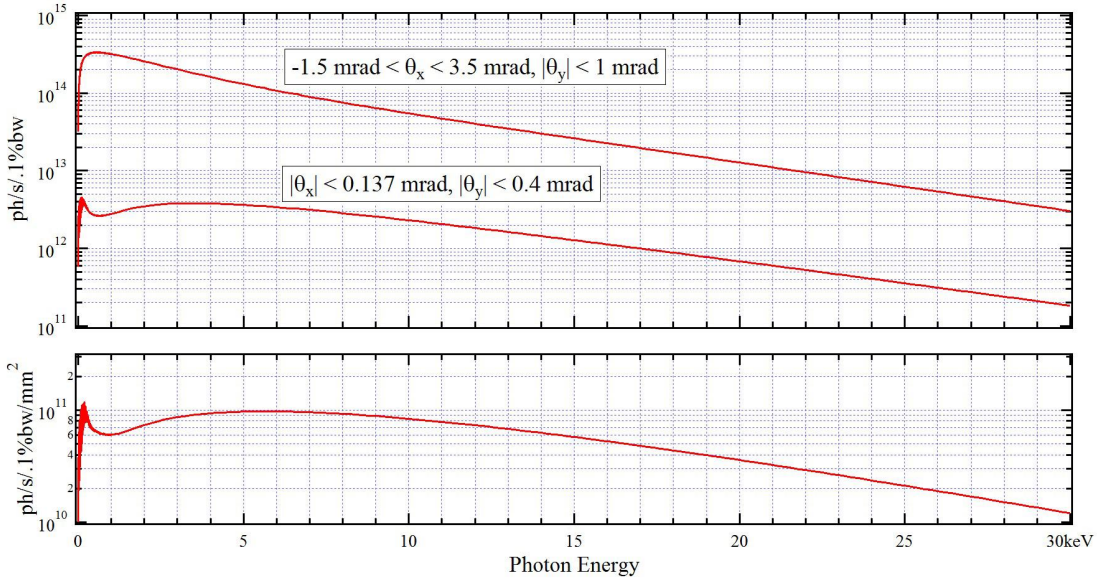

Figure 5. Spectral flux through large and small apertures (two top curves) and the on-axis spectral flux per unit surface area for 30 m observation distance (lower curve) of the 3PW radiation with contribution from bending magnet edges.

The calculated radiation spectral flux collected within different angular limits and the on-axis flux per unit surface area at 30 m observation distance from the 3PW center are presented in figure 5. The angular limits for the highest flux curve (-1.5 mrad $< \theta_x < 3.5$ mrad in the horizontal and $|\theta_y| < 1$ mrad in the vertical plane) correspond to the maximal possible radiation extraction angles due to constraints imposed by the vacuum chamber and the magnets system of NSLS-II. Besides the radiation from the 3PW central pole, radiation from its two side poles, and from bending magnets (in particular the downstream one) contribute to this angular aperture. The angular collection limits of the lower flux curve ($|\theta_x| < 0.137$ mrad, $|\theta_y| < 0.4$ mrad) correspond to the values used at one of 3PW based hard X-ray beamlines of NSLS-II. Even though the horizontal collection angle is small and the flux essentially comes from the 3PW central cone (especially

in the hard X-ray range) in this case, some contribution of radiation from side 3PW poles and bending magnet edges still takes place at low energies (below ~1 keV). Even the on-axis flux per unit surface curve has some contribution of radiation from these "extra" sources in this spectral range; and at very low photon energies (10 - 100 eV) interference of radiation from these sources takes place (see lower graph in figure 5).

Intensity distributions of monochromatic radiation from 3PW and bending magnet edges at different photon energies in the range from 10 eV to 10 keV calculated for 30 m observation distance are presented in figure 6. The distribution at 10 eV (see first image plot on the left) represents a complicated interference pattern of the radiation from different 3PW poles (large interference rings) and from bending magnet edges (so-called "edge radiation" producing smaller interference rings in the center of the image [16]). At 100 eV, the interference effects are still important (with the edge radiation still noticeable in the center of the pattern), though the entire distribution is more collimated, and the contribution of radiation from the side 3PW poles starts to be significant (two emerging "lobes" at horizontal positions 10 mm < |x| < 50 mm). At 1 keV, the contributions from the 3PW side poles dominate the entire intensity distribution. However, at 10 keV (and at higher photon energies) the intensity distribution is essentially dominated by the radiation from the 3PW central pole. At large horizontal positions (|x| > ~50 mm) in the horizontal intensity cuts at all photon energies (see middle-column graphs in figure 6) show contributions of the conventional bending magnet radiation.

The radiation power density distribution (integrated over all photon energies) calculated for 30 m observation distance from the 3PW central pole is shown in figure 7. The shape of the distribution vs horizontal position with two peaks at x ≈ +/-30 mm results from overlapping (incoherent sum) of the radiation from the central and side 3PW poles, as well as from the bending magnets.

We note that the majority of 3PW based beamlines at NSLS-II use the spectral range from ~5 to 25 keV and therefore "see" mainly the radiation from the 3PW central pole, almost without contributions from the side 3PW poles and bending magnets. At higher electron energy rings, contributions from these undesirable sources can however take place at higher photon energies; therefore, e.g. for the ESRF ultra-small emittance upgrade, two more types of IDs are developed for bending magnet type beamlines in addition to the 3PW [42].

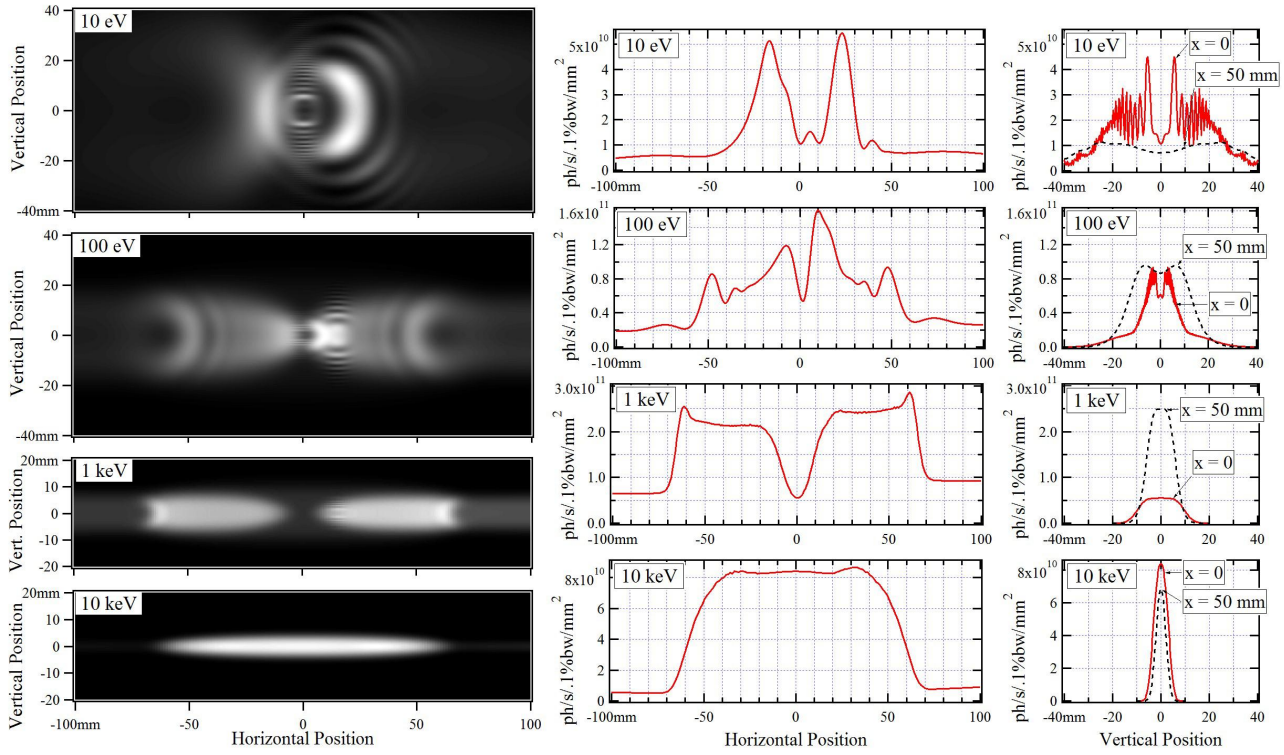

Figure 6. Intensity distributions of 3PW radiation (with contribution from bending magnets) at four different photon energies, for 30 m observation distance. Left column: 2D distributions represented by image plots; central column: intensity in the horizontal mid-plane; right column: intensity cuts by vertical planes at two different horizontal positions, 0 and 50 mm.

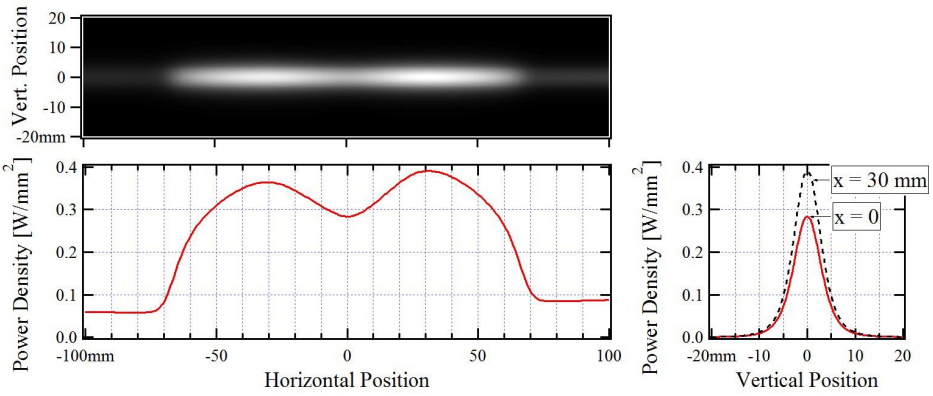

Figure 7. Power density distribution of 3PW radiation (with contribution from bending magnets) for 30 m observation distance. Top: 2D distribution represented by image plot; bottom: power density in the horizontal mid-plane (on the left), and in vertical planes at two different horizontal positions, 0 and 30 mm.

5. CALCULATION EXAMPLES: X-RAY OPTICS, BEAMLINES, EXPERIMENTS

5.1 Development of new beamlines

Optical scheme optimizations and performance estimations for new SR beamlines are among the main areas of applications of the SR emission and propagation simulation codes such as SRW [26], [27], [33], [43], [44]. After the end of construction and start of operation of the first series of NSLS-II beamlines, activities are underway in the scope of subsequent new beamline development projects. One of such projects targets the development of a Coherent Diffraction Imaging (CDI) beamline for the NSLS-II. The optical layout of such a beamline has to ensure most efficient "filtering" of the coherent flux portion from the total hard X-ray flux generated by an undulator, and to allow for an easy change of the radiation spot size and degree of coherence at the sample position, while keeping the radiation beam waist at a desired longitudinal position (in most cases also at the sample). The SRW code, which is entirely based on the physical optics principles, allows for performing such constrained optimization with very high accuracy and at a high level of detail. The current intermediate results obtained by partially-coherent simulations with SRW for the NSLS-II CDI beamline are described in [45].

5.2 Estimating efficiency of X-ray transport optics and impacts of its imperfections on beamline performance

One of important applications of SRW code at NSLS-II is currently the optical performance characterization of beamlines. Besides the tests and eventual correction of undulator spectral performances (see section 4.1), efficiency of X-ray optics can be also easily verified using SRW simulations. An extended work on advanced commissioning and performance characterization of the Coherent Hard X-ray (CHX) beamline of NSLS-II is presented in [46]. Another example of such characterization, using simple comparison of measured X-ray beam characteristics with calculated ones, is described in this section.

A popular optical scheme of high-resolution microscopy beamlines in modern light sources uses intermediate focusing of the X-ray beam by means of mirrors or / and CRL with large focal lengths, and a Secondary Source Aperture (SSA) installed at the position of the intermediate focus, allowing to create a "secondary source" of variable size (eventually much smaller than the size of the electron beam). The radiation from the secondary source is refocused at the sample by a high-resolution final focusing optics. Such a scheme allows for reaching very high, possibly diffraction limited, spatial resolution, while delivering a reasonably high flux to the sample [26]. The presence of such intermediate focus, created with small (or no) demagnification of the original source, allows for realizing very easily useful diagnostics of the electron beam and / or the optics creating this focus. Such simple diagnostics, consisting in measurements of radiation intensity distributions at the intermediate focus and comparison of the measurement results with the corresponding simulations, was realized at the HXN beamline of NSLS-II. It should be noted that at NSLS-II, the use of such diagnostics / tests is particularly important and interesting, because both the horizontal and vertical electron beam emittances can be easily modified. The horizontal emittance can be changed within a factor of ~2 by closing or opening gaps in (all or some of) Damping Wigglers (DW) [47], and the vertical emittance can be changed within a large range by adjusting the coupling, using skew-quadrupole based correction [48].

Measured intensity distributions of 8 keV UR focused near the first SSA location at the HXN beamline (at ~63 m from the undulator center) with the magnification coefficient of ~0.93 are presented in figure 8 (on the left). The measurements were performed with the gaps of all NSLS-II DWs fully open and fully closed. According to the HXN optical scheme, the focusing in the horizontal direction can be performed using two bendable cylindrical mirrors with variable radius of surface curvature, the Horizontal Collimating Mirror (HCM) and the Horizontal Focusing Mirror (HFM). During regular HXN operation, the HCM creates a nearly parallel X-ray beam entering the horizontally-deflecting Dual Crystal Monochromator (DCM) and the HFM focuses the beam after the DCM at the location of SSA. In the measurements under discussion, the HCM surface was made flat, so that the only focusing element in the horizontal direction was the HFM. In the vertical plane, the focusing was performed by CRL (as in usual beamline operation). The size of the horizontal aperture before the HCM was ~1 mm at these measurements, which is smaller than the horizontal size of the UR beam profile at that location; this resulted in only partial illumination of the HCM and HFM.

As one can see from figure 8, the measured radiation spot has larger, ~162 μm Full Width at Half Maximum (FWHM), horizontal size when the DW gaps are open, and smaller, ~134 μm FWHM size, when the DW gaps are closed. SRW simulations, performed for the optical configuration used for these measurements, at the assumption of error-free surfaces of HCM, HFM and DCM crystals, predicted somewhat smaller horizontal spot sizes: ~135 μm FWHM with DW gaps open and ~90 μm FWHM with DW gaps closed, see image plots and graphs on the right in figure 8. For these calculations, the results of the electron beam emittance measurements obtained using the standard NSLS-II diagnostics tool, a pinhole camera, were used. According to the pinhole camera data, the horizontal electron beam emittance was ~2.1 nm with DW gaps open and ~0.9 nm with DW gaps closed. Also, the calculations used the nominal (1.84 m) value of the horizontal beta-function in the center of the low-beta straight section of NSLS-II, where the HXN IVU is installed.

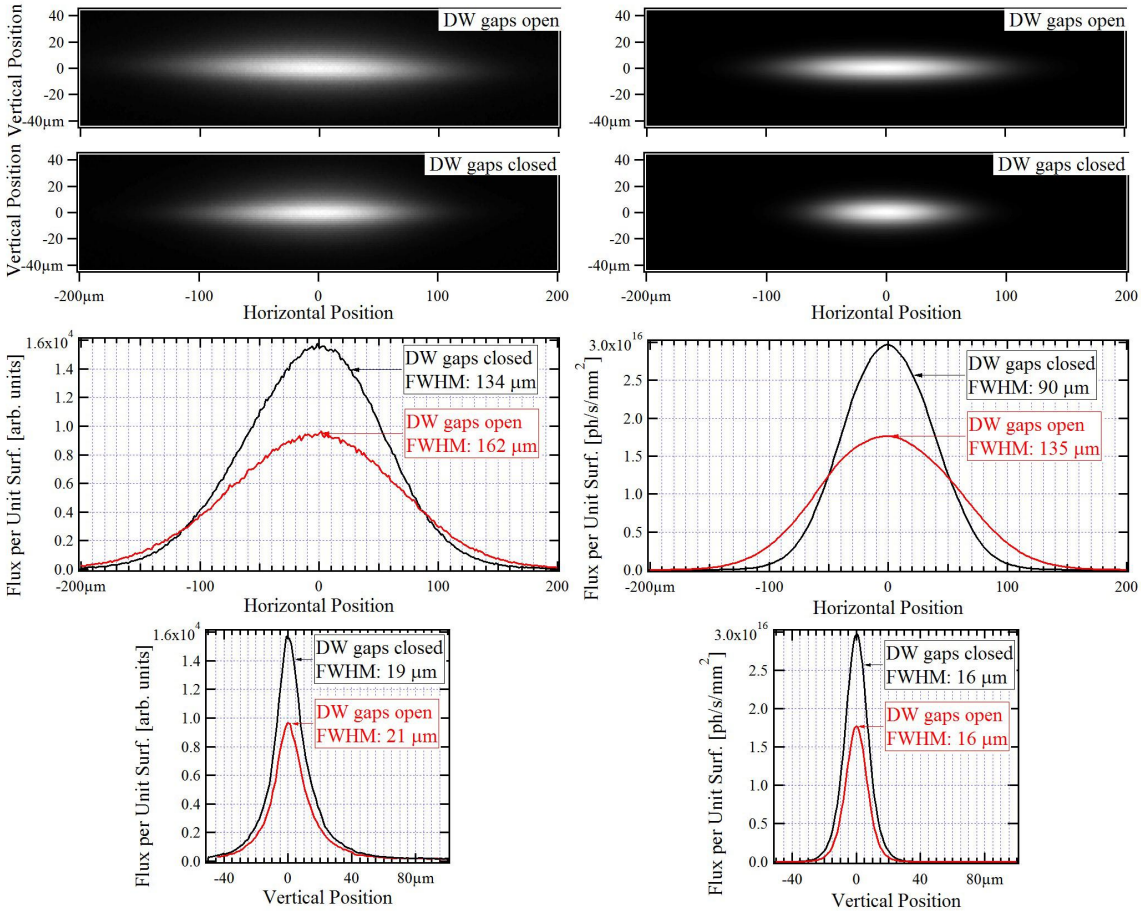

Figure 8. Measured (on the left) and calculated (on the right) intensity distributions of the focused 8 keV UR at HXN beamline near the first SSA location (~63 m from undulator) for the DW gaps open and closed. Graphs in the middle and at the bottom show cuts of the 2D distributions by the horizontal and vertical planes passing through the intensity maxima.

The ratios of the measured-to-calculated horizontal spot sizes are ~1.2 in the case of the open DW gaps and ~1.5 in the case of the closed DW gaps, i.e. the discrepancy between the measured and calculated horizontal focused spot sizes is stronger in the case of the smaller horizontal electron beam emittance (and the electron beam size). This, together with the pinhole camera data, suggests that the observed discrepancy is likely to be explained by imperfections of X-ray optics – surfaces of HCM, HFM and / or possibly DCM crystals. Several additional test simulations performed taking into account HCM and HFM surface height profiles obtained from the optical metrology data could not fully explain the discrepancy with the measurements. Unfortunately, reliable crystal surface height profile data was not available for the use in the simulations. We note that the imperfect focusing of the X-ray beam at the SSA may result in a reduction of the flux at the sample, and so have an impact on beamline performance. Therefore, further experimental and numerical analysis of the existing optical imperfections of the transport optics is planned.

5.3 Simulation of user experiments

The physical optics methods used in the SRW code for the simulation of fully- and partially-coherent radiation propagation through X-ray optical systems can be readily used for the description of processes taking place in some experiments with X-rays in such areas as coherent scattering, coherent diffractive imaging, high-resolution microscopy and others. A possibility of simulating experiments from source to detector at light source facilities has a number of potential benefits. E.g. with such simulations, one can better estimate the feasibility of an experiment with a given sample with a required resolution at a particular beamline; optimal X-ray optics and detector settings (ID gap and crystal angles, slit sizes, mirror radii of curvature, CRL configurations, exposure times, etc.) can be found for the given sample before the experiment, and so less beam time will have to be spent on auxiliary measurements / tests during the actual experiment; experimental data processing algorithms can be tested and tuned, using simulated experimental data, long before actual measurements; impacts of miscellaneous electron beam and X-ray optics instabilities on the quality of experimental data can be studied, etc. The work on simulations of coherent scattering experiments at partially-coherent illumination of samples that are performed at the CHX beamline of NSLS-II is currently in progress. Recent new results, including simulations and measurements of partially coherent X-ray scattering from lithographically created samples with sub-100 nm size objects are reported in [49].

6. SUMMARY

An overview of functions implemented in the SRW code for calculation of different types of SR, and for the simulations of fully- and partially-coherent radiation propagation, using the methods of physical optics, was presented, together with several examples of the simulations related to development and commissioning of IDs and X-ray optics for modern light source facilities. Thanks to the generality and accuracy of calculation methods implemented in the code, the areas of its applications keep increasing in number, covering now not only the development of sources and X-ray optics, but also complete simulation of some types of experiments. The continuously increasing radiation coherence in new generations of light source facilities makes the simulations using the methods implemented in SRW more and more practically important, and also more often more feasible and easy numerically. Collaborative development of the code, including its core part and interfaces, is still in progress, aiming to further extend the library of physical optics propagators and utilities for the simulation of X-ray optics and experimental samples, improve CPU-efficiency and parallelization of partially-coherent calculations, and simplify the practical use of the code on computer systems of different scale.

ACKNOWLEDGMENTS

We would like to thank contributors to SRW, users and supporters of this code, in particular D. L. Bruhwiler, R. Nagler, P. Moeller (RadiaSoft), J. Sutter, D. Laundy, K. Sawhney (Diamond Light Source) L. Samoylova, A. Buzmakov, S. Yakubov (European XFEL), J. Krzywinski, L. Zhang, C.C. Kao (SLAC), G. Williams, J. Thieme, T. Tanabe, A. Blednykh, T. Shaftan and Q. Shen (NSLS-II, BNL). The work was supported by US DOE contract DE-SC0012704 and SBIR grant DE-SC0011237.

REFERENCES

[1] Borland, M., "Elegant: a flexible SDDS-compliant code for accelerator simulation," Advanced Photon Source LS-287 (2000).

[2] Bengtsson, J., "Tracy-2 User's Manual" (1997).
[3] Eriksson, M., Lindgren, L.-J., Sjöström, M., Wallén, E., Rivkin, L., Streun, A., "Some small-emittance light-source lattices with multi-bend achromats," Nucl. Instrum. and Methods A587 (2-3), 221-226 (2008).
[4] Borland, M., Decker, G., Emery, L., Sajaev, V., Sun, Y., Xiao, A., "Lattice design challenges for fourth-generation storage-ring light sources," J. Synchrotron Rad. 21, 912-936 (2014).
[5] Carmignani, N., Farvacque, L., Liuzzo, S. M., Nash, B., Perron, T., Raimondi, P., Versteegen, R., White, S., "Linear and nonlinear optimizations for the ESRF upgrade lattice," Proc. IPAC-2015, TUPWA013, 1422-1425 (2015).
[6] Bruns, W., "The GdfidL electromagnetic field simulator"; http://www.gdfidl.de
[7] Chubar, O., Elleaume, P. and Chavanne, J., "A 3D magnetostatics computer code for insertion devices," J. Synchrotron Rad. 5, 481-484 (1998).
[8] Walker, R. P., Diviacco, B., "URGENT: software code for insertion devices," Sincrotrone Trieste, Italy (1990).
[9] Chubar, O. and Elleaume, P., "Accurate and efficient computation of synchrotron radiation in the near field region," Proc. EPAC-98, 1177-1179 (1998).
[10] Tanaka, T. and Kitamura, H., "SPECTRA: a synchrotron radiation calculation code," J. Synchrotron Rad. 8, 1221-1228 (2001).
[11] Scheer, M., "WAVE - a computer code for the tracking of electrons through magnetic fields and the calculation of spontaneous synchrotron radiation," Proc. ICAP-2012, TUACC2, 86-88 (2012).
[12] Del Rio, M. S., Canestrari, N., Jiang, F. and Cerrina, F., "SHADOW3: a new version of the synchrotron X-ray optics modelling package," J. Synchrotron Rad. 18 (5), 708-716 (2011).
[13] Schäfers, F., "The BESSY raytrace program RAY," in [Modern developments in X-ray and neutron optics], Springer Series in optical science 137, 9-41 (2008).
[14] Prodi, A., Knudsen, E., Willendrup, P., Schmidt, S., Ferrero, C., Lefmann, K. et al. "A monte carlo approach for simulating the propagation of partially coherent X-ray beams," Proc. SPIE 8141, 814108 (2011).
[15] Shi, X., Reininger, R., del Rio, M. S. and Assoufid, L., "A hybrid method for X-ray optics simulation: combining geometric ray-tracing and wavefront propagation," J. Synchrotron Rad. 21 (4), 669-678 (2014).
[16] Chubar, O., "Precise computation of electron beam radiation in non-uniform magnetic fields as a tool for the beam diagnostics," Rev. Sci. Instrum. 66 (2), 1872-1874 (1995).
[17] Chubar, O., Berman, L., Chu, Y. S., Fluerasu, A., Hulbert, S., Idir, M., Kaznatcheev, K., Shapiro, D., Shen, Q., Baltser, J., "Development of partially-coherent wavefront propagation simulation methods for 3rd and 4th generation synchrotron radiation sources," Proc. SPIE 8141, 814107 (2011).
[18] Chubar, O., Couprie, M.-E., Labat, M., Lambert, G., Polack, F., Tcherbakoff, O., "Time-dependent FEL wavefront propagation calculations: Fourier optics approach," Nucl. Instrum. and Methods A593, 30-34 (2008).
[19] Sutter, J. P., Chubar, O., Suvorov, A., "Perfect crystal propagator for physical optics simulations with Synchrotron Radiation Workshop," Proc. SPIE 9209, 92090L (2014).
[20] Zachariasen, W. H., [Theory of X-Ray Diffraction in Crystals], John Wiley & Sons, New York (1945).
[21] Nazaretski, E., Lauer, K., Yan, H., Bouet, N., Zhou, J., Conley, R., Hang, X., Xu, W., Lu, M., Gofron, K., Kalbfleisch, S., Wagner, U., Rau, C., Chu, Y. S., "Pushing the limits: an instrument for hard X-ray imaging below 20 nm," J. Synchrotron Rad. 22, 336-341 (2015).
[22] Roling, S., Zacharias, H., Samoylova, L., Sinn, H., Tschentscher, T., Chubar, O., Buzmakov, A., Schneidmiller, E., Yurkov, M. V., Siewert, F., Braun, S. and Gawlitza, P., "Time-dependent wave front propagation simulation of a hard X-ray split-and-delay unit: towards a measurement of the temporal coherence properties of X-ray free electron lasers," Phys. Rev. ST Accel. Beams 17, 110705 (2014).
[23] Chubar, O., Geloni, G., Kocharyan, V., Madsen, A., Saldin, E., Serkez, S., Shvyd'ko, Y., Sutter, J., "Ultra-high-resolution inelastic X-ray scattering at high-repetition-rate self-seeded X-ray free-electron lasers," J. Synchrotron Rad. 23, 410-424 (2016).
[24] Chubar, O., Elleaume, P., Kuznetsov, S., Snigirev, A., "Physical optics computer code optimized for synchrotron radiation," Proc. SPIE 4769, 145-151 (2002).
[25] Weitkamp, T., Chubar, O., Drakopoulos, M., Snigireva, I., Snigirev, A., Schroer, C., Guenzler, F., Lengeler, B., "Refractive lenses as a beam diagnostics tool for high-energy synchrotron radiation," Nucl. Instrum. and Methods A467-468, 248-251 (2001).
[26] Chubar, O., Chu, Y. S., Kaznatcheev, K., Yan, H., "Application of partially coherent wavefront propagation calculations for design of coherence-preserving synchrotron radiation beamlines," Nucl. Instrum. and Methods A649 (1), 118-122 (2011).

[27] Fluerasu, A., Chubar, O., Kaznatcheev, K., Baltser, J., Wiegart, L., Evans-Lutterodt, K., Carlucci-Dayton, M., Berman, L., "Analysis of the optical design of the NSLS-II coherent hard X-ray beamline," Proc. SPIE 8141, 81410J (2011).
[28] http://fftw.org
[29] https://github.com/ochubar/SRW
[30] https://www.wavemetrics.com
[31] http://www.esrf.eu/Accelerators/Groups/InsertionDevices/Software/SRW
[32] https://docs.python.org/2/c-api/index.html; https://docs.python.org/3/c-api/index.html
[33] Chubar, O., "Recent updates in the Synchrotron Radiation Workshop code, on-going developments, simulation activities, and plans for the future," Proc. SPIE 9209, 920907 (2014).
[34] http://pythonhosted.org/mpi4py
[35] Rakitin, M., Chubar, O., Moeller, P., Nagler, R., Bruhwiler, D. L., "Sirepo: a web-based interface for physical optics simulations – its deployment and use at NSLS-II," these proceedings.
[36] https://jupyter.org
[37] Samoylova, L., Buzmakov, A., Chubar, O., Sinn, H., "WavePropaGator: interactive framework for X-ray free-electron laser optics design and simulations," J. Appl. Crystallogr. 49 (4), 1347-1355 (2016).
[38] Benabderrahmane, C. et al., "Development and operation of a Pr2Fe14B based cryogenic permanent magnet undulator for a high spatial resolution X-ray beamline," arXiv:1612.03748v1 [physics.acc-ph] (2016).
[39] Chubar, O., Chu, Y. S., Huang, X. J., Kalbfleisch, S., Yan, H., Shaftan, T., Wang, G., Cai, Y. Q., Suvorov, A., Fluerasu, A., Wiegart, L., Chen-Wiegart, Y.-c.K., Thieme, J., Williams, G., Idir, M., Tanabe, T., Zschack, P., Shen, Q., "Initial performances of first undulator-based hard X-ray beamlines of NSLS-II compared to simulations," Proc. SRI-2015, AIP Conf. Proc. 1741, 040002 (2016).
[40] Halbach, K., "Permanent Magnet Undulators," J. Physique, C1, Suppl.2, 44 (1983).
[41] Tanabe, T., Kitegi, C., He, P., Musardo, M., Chubar, O., Rank, J., Cappadoro, P., Fernandes, H., Harder D., Corwin, T., "The latest status of NSLS-II insertion devices," Proc. Pan-Am. SRI-2013, J. Phys.: Conf. Ser. 493, 012031 (2014).
[42] Chavanne, J., "Implementation of short wigglers as photon sources for the bending magnet beamlines in the new ESRF lattice," ESRF 01-15/IDM/v.0 (2015).
[43] Canestrari, N., Bisogni, V., Walter, A., Zhu, Y., Dvorak, J., Vescovo, E., Chubar, O., "Wavefront propagation simulations for a UV/soft X-ray beamline: Electron Spectro-Microscopy beamline at NSLS-II," Proc. SPIE 9209, 92090I (2014).
[44] Suvorov, A., Cai, Y. Q., Sutter, J. P., Chubar, O., "Partially-coherent wavefront propagation simulations for inelastic X-ray scattering beamline including crystal optics," Proc. SPIE 9209, 92090H (2014).
[45] Williams, G., Robinson, I., Chubar, O., Berman, L., Chu, Y. S., "Optical design and simulation of a new coherence beamline at NSLS-II," these proceedings.
[46] Wiegart, L., Rakitin, M., Fluerasu, A., Chubar, O., "X-ray optical simulations supporting advanced commissioning of the coherent hard X-ray beamline at NSLS-II," these proceedings.
[47] Wang, G. et al., "NSLS-II storage ring insertion device and front-end commissioning and operation," Proc. SRI-2015, AIP Conf. Proc. 1741, 020044 (2016).
[48] Li, Y., Yang, L., Cheng, W., "Characterization and control of linear coupling using turn-by-turn beam position monitor data in storage rings," arXiv:1706.06022 [physics.acc-ph] (2017).
[49] Chubar, O., Rakitin, M., Chen-Wiegart, Y.-c. K., Fluerasu, A., Wiegart, L., "Simulation of experiments with partially-coherent x-rays using Synchrotron Radiation Workshop," these proceedings.